International Journal of Biological Macromolecules 327 (2025) 146558

Contents lists available at ScienceDirect

International Journal of Biological Macromolecules

journal homepage: www.elsevier.com/locate/ijbiomac

Beyond plasma membrane disruption: Novel antifungal mechanism of *Neosartorya* (*Aspergillus*) *fischeri* antifungal protein 2 in *Candida albicans*

Kinga Dán [a,b], Nóra Zsindely [c], Zoltán Kele [d], Krisztián Laczi [a], John K. Karemera [a,b], Csaba Papp [a], Attila Farkas [e], Gergely Maróti [e], Attila Borics [f], László Bodai [c], László Galgóczy [a,*]

[a] Department of Biotechnology and Microbiology, Faculty of Science and Informatics, University of Szeged, Közép fasor 52, H-6726 Szeged, Hungary
[b] Doctoral School of Biology, Faculty of Science and Informatics, University of Szeged, Közép fasor 52, H-6726 Szeged, Hungary
[c] Department of Biochemistry and Molecular Biology, Faculty of Science and Informatics, University of Szeged, Közép fasor 52, H- 6726 Szeged, Hungary
[d] Department of Medical Chemistry, Albert Szent-Györgyi Medical School, University of Szeged, Dóm tér 8, H-6720 Szeged, Hungary
[e] Institute of Plant Biology, HUN-REN Biological Research Centre, Temesvári krt. 62, H-6726 Szeged, Hungary
[f] Institute of Biochemistry, HUN-REN Biological Research Centre, Temesvári krt. 62, H-6726 Szeged, Hungary

ARTICLE INFO

Keywords:
Candida albicans
Neosartorya (*aspergillus*) *fischeri* antifungal protein 2
Transcriptome
Protein target
Antifungal mechanism

ABSTRACT

Candida albicans is the most common human fungal pathogen and one of the major causes of drug-resistant, life-threatening fungal infections. The *Neosartorya* (*Aspergillus*) *fischeri* antifungal protein 2 (NFAP2), exhibits potent antifungal activity in both planktonic and biofilm-forming *Candida* cells *in vitro* and *in vivo*. However, the exact antifungal mechanism of NFAP2 remains unelucidated, limiting its therapeutic application. Based on our observations, we posit that NFAP2 is internalized in *Candida* cells and slows the growth over time, in addition to its previously characterized rapid plasma membrane disruption effect.

This study aimed to understand the molecular mechanism of the long-term growth-slowing effect of NFAP2 on *C. albicans*. Transcriptomic analyses indicated downregulation of genes involved in metabolism and upregulation of genes associated with the cell cycle and filamentous growth. Moreover, *in vivo* protein–protein interaction analysis identified glutamate decarboxylase (Gad1p), ATP synthase subunit alpha (Atp1p), and enolase 1 (Eno1p) as intracellular protein targets of NFAP2.

Our results support a dual mechanism of action of NFAP2. Specifically, when NFAP2 is applied below the minimum inhibitory concentration (<MIC), it enters the cells and reduces the metabolic activity by interacting with Gad1p, Atp1p, and Eno1p, resulting in slow growth. Furthermore, NFAP2 induces the yeast−hypha transition. However, when NFAP2 is applied at the MIC, it rapidly disrupts the plasma membrane.

1. Introduction

Over the past decade, several epidemiological surveys have highlighted the increasing number of fungal infections [1–3]. Based on the most recent surveys, >6.5 million people are affected by life-threatening fungal infections each year, resulting in approximately 3.8 million deaths. This is mainly due to poor diagnoses, the increasing number of antifungal drug-resistant strains, and the lack of effective antifungal therapy [4–7]. In response, the World Health Organization (WHO) published the first-ever Fungal Priority Pathogens List (FPPL) in October 2022. This initiative was the first global attempt to systematically prioritize the most significant fungal pathogens, categorizing them into following three priority groups: critical, high, and medium [8]. *Candida albicans* is included in the critical group because it is the most prevalent human pathogenic fungus. Furthermore, it has been responsible for a growing number of drug-resistant and fatal invasive infections over the past two decades [4,9,10].

In light of the global antifungal crisis, the WHO FPPL recommends immediate interventions and strategies to control fungal infections and mitigate the development of antifungal resistance. One of the objectives is to encourage researchers to discover new antifungal drugs [8]. In this regard, antifungal proteins (AFPs) secreted by filamentous fungi belonging to the class Eurotiomycetes represent promising new compounds for controlling fungal infections. Interestingly, the majority of these AFPs share common characteristics, *i.e.*, low molecular weight, water solubility, and a cationic nature. They also have a compact

* Corresponding author at: Department of Biotechnology and Microbiology, Faculty of Science and Informatics, University of Szeged, Szeged, Hungary.
E-mail address: galgoczi@bio.u-szeged.hu (L. Galgóczy).

https://doi.org/10.1016/j.ijbiomac.2025.146558
Received 30 May 2025; Received in revised form 21 July 2025; Accepted 2 August 2025
Available online 21 August 2025

β-folded tertiary structure, which is stabilized by three to four intramolecular disulfide bonds between the cysteine residues. Thus, they are highly stable in harsh environmental conditions and resistant to proteolysis [11,12]. Furthermore, AFPs exhibit a broad antifungal spectrum [13], making them effective against both molds and yeasts [11,14]. According to our previous studies, one of the most effective anti-yeast AFPs is *Neosartorya* (*Aspergillus*) *fischeri* antifungal protein 2 (NFAP2). It is secreted by the isolate *N.* (*A.*) *fischeri* NRRL 181. NFAP2 effectively inhibits the growth of both planktonic and sessile (biofilm-forming) cells of *C. albicans* [15,16]. Furthermore, it exhibits synergy with conventional antifungal drugs upon *in vitro* [17] and *in vivo* combined application [16]. Markedly, NFAP2 is non-toxic to human cell lines and mice, and effectively inhibits the growth of *C. albicans* in fluconazole-resistant murine vulvovaginitis [16], and three-dimensional skin infection models [18]. Microevolutionary studies have demonstrated that resistance development to NFAP2 occurs at a significantly lower frequency than to fluconazole, underscoring the long-term therapeutic potential of NFAP2 [19]. Collectively, these attributes position NFAP2 as a promising alternative antifungal drug, particularly for the management of superficial drug-resistant *C. albicans* infections, and support its further development for clinical application.

Therapeutic application of NFAP2 requires understanding its antifungal mechanisms in *C. albicans*, which remain unelucidated thus far. Our previous studies show that NFAP2 disrupts the plasma membrane integrity of *C. albicans* cells when treated with a relatively high NFAP2 concentration [16,17]. This is most likely due to the selective interaction with the negatively charged fungal cell membrane [20].

In the present study, we show that the antifungal mechanism of NFAP2 is more complex than a 'simple' plasma membrane disruption, because it can be internalized by *C. albicans* cells and causes a significant reduction in cell growth. Thus, our main objective was to understand this antifungal mechanism. Transcriptome data indicated enhanced hyphal growth and disturbances in energy and carbon metabolism in *C. albicans* cultures grown in the presence of NFAP2. The plausible mechanism underlying this was further evidenced by *in vivo* protein–-protein interaction analysis. These results were used to identify glutamate decarboxylase, ATP synthase subunit alpha, and enolase 1 as intracellular protein targets of NAFP2.

2. Materials and methods

2.1. NFAP2 production

Recombinant NFAP2 was produced in a *Penicillium chrysogenum*-based expression system and purified using cation exchange and reversed-phase high-performance liquid chromatography to achieve near 100 % purity, as described previously [16,17,21].

2.2. Confocal laser scanning microscopy (CLSM)

C. albicans SC5314 cells (2×10^7 cells mL^{-1}) were treated with 3.125 μg mL^{-1} green fluorophore boron-dipyrromethene-labeled (BODIPY) NFAP2 (Bd-NFAP2) for 30, 60, 120, and 240 min in low ionic strength medium [LCM: 0.5 % glucose, 0.25 % yeast extract, 0.0125 % peptone (*w/v*)] at 30 °C with continuous shaking at 160 rpm. After incubation, the samples were stained with 5 μg mL^{-1} Fluorescent Brightener 28 (FB28; VWR International, Radnor, PA, USA) for 10 min and 5 μg·mL^{-1} propidium-iodide (PI; Sigma-Aldrich, St. Louis, MO, USA) for 5 min at room temperature in the dark. After washing with phosphate-buffered saline (PBS), the samples were mounted onto microscope slides, covered with 2 % (*w/v*) agar slices, and examined using an Olympus Fluoview FV 1000 confocal laser microscope with 60× magnification (Olympus, Shinjuku, Japan). A 488-nm laser was used for excitation. The excitation and emission wavelengths were 380 nm and 475 nm for FB28, 504 nm and 512 nm for Bd-NFAP2, and 535 nm and 617 nm for PI, respectively. Sequential scanning was used to avoid crosstalk between the fluorescent dyes.

2.3. Fluorescence-activated cell sorting (FACS)

C. albicans SC5314 cells were diluted in LCM (2×10^7 cells·mL^{-1}) and treated with 7.5 μg mL^{-1} and 15 μg mL^{-1} Bd-NFAP2 for 6 h at 30 °C with continuous shaking at 160 rpm and counterstained with PI as described above. Untreated cells served as the negative fluorescence control, whereas cells treated with 70 % (*v/v*) ethanol (10 min at room temperature, 160 rpm shaking) were used as the positive control for PI staining as well as the calibration control. Cells were treated with 2 μg mL^{-1} fluorescein diacetate (Thermo Fischer Scientific, Waltham, MA, USA) for 20 min at room temperature with continuous shaking at 160 rpm and used as calibration controls for the Bd-NFAP2-treated samples. Subsequently, cells were washed in PBS and collected using centrifugation at 9000 ×*g* for 5 min. Bd-NFAP2- and PI-positive cells were counted using a FlowSight imaging flow cytometer (Amins, Merck Millipore, Billerica, MA, USA). A minimum of 10,000 cells were counted per run. The Image Data Exploration and Analysis software (IDEAS; Amins, Millipore) was used for data analysis. The gating was adjusted to visualize at least 96 % of the untreated cells, and debris was excluded during data acquisition. Experiments were performed in independent duplicates. Pearson's chi-squared test and the Phi coefficient were used to calculate statistically significant differences ($p \leq 0.05$) among PI+, Bd-NFAP2+, Double+, and all Bd-NFAP2+ cells following treatment with varying concentrations of NFAP2 (Statistic Kingdom online platform, 2025; https://www.statskingdom.com/310GoodnessChi.html).

2.4. Effect of NFAP2 on the growth rate of C. albicans culture

The growth rate of *C. albicans* in response to NFAP2 treatment was evaluated by comparing the cell densities of the cultures treated with NFAP2 at the minimum inhibitory concentration (MIC), at 15 μg·mL^{-1}, and at 7.5 μg·mL^{-1}, and comparing them to untreated controls cultures. Mid-log phase *C. albicans* SC5314 cells from an overnight culture (10 mL LCM, 30 °C, 160 rpm) were diluted to 2×10^7 cells mL^{-1} in 40 mL LCM, supplemented with 7.5 μg mL^{-1}, 15 μg mL^{-1} and 200 μg mL^{-1} (MIC) NFAP2 and incubated for 6 h at 30 °C with continuous shaking at 160 rpm. Culture without NFAP2 supplementation served as the untreated control. Cell densities (OD_{600}) of the cultures were measured every 30 min using a Genesys 150 UV–Visible Spectrophotometer (Thermo Fisher Scientific). To test growth ability following the incubation period, a fivefold serial dilution was prepared from each culture using the same medium. Subsequently, 5 μL of each dilution was spotted onto yeast extract-peptone-dextrose medium [YPD: 1 % yeast extract, 2 % peptone, 2 % D-glucose (*w/v*)] agar plates, allowed to dry, and incubated at 30 °C for 24 h.

2.5. RNA isolation

For RNA isolation, mid-log phase *C. albicans* SC5314 cells, untreated or treated with NFAP2 (15 μg mL^{-1}), were used as described above for the growth rate investigation protocol. The NFAP2-treated cultures were incubated for 6 h at 30 °C under continuous shaking at 160 rpm, whereas untreated controls were incubated for 2 h under the same conditions. After incubation, the cells were collected using centrifugation (1000 ×*g*, 5 min), washed with PBS, frozen in liquid nitrogen, and stored at −80 °C until RNA isolation. Three independent biological replicates were used for RNA isolation. Total RNA was purified using the *Quick*-RNA Plant Miniprep Kit (Zymo Research, Tustin, CA, USA) according to the manufacturer's instructions. The quantity and quality of the isolated RNA were assessed using a NanoDdrop ND-1000 spectrophotometer (Thermo Fisher Scientific), agarose gel electrophoresis, and the 2100 BioAnalyzer electrophoresis system (Agilent Technologies, Santa Clara, CA, USA).

2.6. RNA sequencing and transcriptome analysis

Poly(A)-RNA species were first purified from the total RNA samples using the NEBNext Poly(A) mRNA Magnetic Isolation Module (New England Biolabs, Ipswich, MA, USA); then barcoded, strand-specific RNA-sequencing libraries were generated using NEBNext Ultra II Directional RNA Library Prep with the Sample Purification Beads kit (New England Biolabs) and NEBNext Multiplex Oligos for Illumina (New England Biolabs). The fragment length distribution and DNA concentration of the RNA-sequencing libraries were determined using capillary gel electrophoresis using the 2100 Bioanalyzer with the DNA 1000 kit (Agilent Technologies). Sequencing-libraries were pooled in equimolar concentrations, denatured in 0.1 M NaOH, and sequenced using two replicate sequencing runs with a MiSeq DNA sequencer (Illumina, San Diego, CA, USA) using the MiSeq Reagent Kit v3–150 (Illumina). Primary sequence analysis (*i.e.*, image analysis, base-calling, fastq file generation, demultiplexing) was performed using the on-board MiSeq Control Software v. 2.6.2.1 and the Real-Time Analysis software v. 1.18.54.

In this study, transcriptome analysis was performed using the CLC Genomics Workbench 21.0.3 (https://digitalinsights.qiagen.com/). The reads were quality-trimmed and mapped using the *C. albicans* SC5314 genome sequence. Differential expression analysis was performed by comparing the NFAP2-treated samples with the untreated ones. The threshold for the upregulated genes was set to $\log_2$ fold-change >1.5, whereas that for the downregulated genes was set to $\log_2$ fold-change< −1.5. Only gene expression changes with a $p < 0.05$ were considered significant. Moreover, gene ontology (GO) and Kyoto encyclopedia of genes and genomes (KEGG) pathway enrichment analysis was performed with the database for annotation, visualization, and integrated discovery (DAVID) web server (https://davidbioinformatics.nih.gov/) [22,23]. Figures were generated using R version 4.3.3 in conjunction with the ggplot2 package version 3.5.1 [24].

2.7. Identification of intracellular soluble protein interaction partners of NFAP2 in C. albicans

C. albicans SC5314 cells from an overnight (10 mL LCM, 30 °C, 160 rpm) culture were diluted to 2×10^9 cells mL^{-1} in LCM and treated with 50 μg mL^{-1} NFAP2 for 4 h at 30 °C with continuous shaking at 160 rpm. Cells were then washed twice with 1 mL ice-cold PBS (1000 ×*g*, 5 min) and resuspended in PBS. The cell suspension was treated with 1.25 mM succinimidyl 2-(4,4′-azipentanamido)ethyl-1,3′-dithiopropionate (NHS-SS-Diazirine, SDAD) (Thermo Fisher Scientific), and subsequently exposed to UV irradiation (365 nm, 5 cm, 12 min) to stabilize the protein–protein interactions. After UV irradiation, the cells were suspended in 900 μL PBS and the total soluble protein was extracted.

Glass beads (0.7 g, 1.0 mm diameter) were also added to the cell suspension and incubated at −80 °C for 5 min. The cells were then disrupted with Tissue Lyzer (Qiagen, Hilden, Germany) at 50 Hz for 3 min and incubated at −80 °C for 5 min. These steps were repeated 20 times [25]. After this disruption process, the suspension was centrifuged (1000 ×*g*, 5 min) to separate the soluble proteins from the cell debris and beads. Protein concentration was measured with the Qubit Protein Assay Kit (Thermo Fisher Scientific), while the NFAP2-interacting proteins were enriched using Protein G Plus-Agarose (Santa Cruz Biotechnology, Dallas, TX, USA), based on the manufacturer's instructions.

Briefly, 10 μL NFAP2 antibody solution (1.13 mg mL^{-1}; produced in rabbit; Davids Biotechnologie GmbH, Regensburg, Germany) was mixed with 400 μL total protein extract (~140 μg mL^{-1}) and incubated at 4 °C for 1 h on a rotating device. Then, 20 μL Protein G Plus-Agarose solution was added to the mixture, incubated at 4 °C overnight on a rotating device, and centrifuged and washed with PBS three times (6000 ×*g*, 5 min, 4 °C). The pellet was resuspended in 32 μL ddH_2O and 8 μL Pierce™ Lane Marker Non-Reducing Sample Buffer (Thermo Fisher Scientific) and heated at 70 °C for 5 min. A 12 % (*w/v*) SDS-PAGE was used (20 μL sample/well) to separate the enriched proteins according to their molecular weights. In this case, protein bands were visualized with Coomassie Brilliant Blue R-250 staining. Western blotting was applied to identify the proteins interacting with NFAP2. After washing the protein gel and the membrane in the transfer buffer (48 mM Tris, 39 mM glycine, 20 % (*v/v*) methanol, 1.3 mM SDS pH = 9.20) for 5 min at 45 rpm, the separated proteins were transferred to a 0.45 μm nitrocellulose membrane (Thermo Fisher Scientific) using a semi-dry blotting system (TransBlot® SD Semi-Dry Electrophoretic Transfer Cell; Bio-Rad Laboratories, Hercules, CA, USA) at 25 V for 45 min. The membrane was then blocked in 3 % (*w/v*) fat-free milk powder in a PBS-T (PBS supplemented with 0.1 % (*v/v*) Tween-20) for 2 h at 45 rpm. The blocked membrane was incubated overnight at 4 °C in 1 % (*w/v*) fat-free milk powder in a PBS-T containing antigen affinity-purified NFAP2 polyclonal antiserum (1.13 mg mL^{-1}; produced in rabbit; Davids Biotechnologie GmbH) at a 1:1000 ratio.

Finally, the membrane was washed three times in PBS-T for 10 min at 45 rpm. The membrane was incubated in 1 % (*w/v*) fat-free milk powder in PBS-T containing Anti-Rabbit IgG (whole molecule)–Peroxidase antibody produced in goat (Thermo Fisher Scientific) at a 1:10000 ratio for 1 h at 45 rpm. After three washings in PBS-T (10 min, 45 rpm), the membrane was washed with ddH_2O for 5 min at 45 rpm and then incubated in a substrate buffer (1 M Tris HCl pH = 8.3, 5 M NaCl, 1 M $MgCl_2$) for 1 min at 45 rpm. Overall, detection was performed with 1-Step NBT/BCIP solution (Thermo Fisher Scientific) and stopped with ddH_2O. The bands corresponding to the detected proteins in the membrane were excised and mass spectrometry (MS) analysis was performed. The protein extract of *C. albicans* cells without NFAP2-treatment served as a control to exclude non-specific Protein G Plus-Agarose interaction and antibody binding.

2.8. Mass spectrometry

The protein band of interest was carefully excised from the gel, cut into smaller pieces, and placed into a microcentrifuge tube. Proteins in the gel particles were treated using the following in-gel digestion method. First, the samples were rinsed with 0.1 M NH_4HCO_3 solution in MeCN (acetonitrile)/water to remove Coomassie blue from the gel pieces. Among all the washing and reaction steps, MeCN was added to dehydrate the gel pieces, while aqueous NH_4HCO_3 was added to rehydrate them, in the reduction, alkylation, and digestion steps. Second, the possible disulfide bridges were reduced by incubation at 60 °C for 30 min in 100 mM DTT (dithiothreitol) in 0.1 M NH_4HCO_3 solution, after which a 200 mM iodo-acetamide (IAA) solution was added to alkylate the proteins and incubated for an additional 30 min in the dark at room temperature. Finally, the rinsed gel pieces were rehydrated by adding trypsin solution in aqueous 0.1 M NH_4HCO_3 to the tube, after which they were incubated overnight at 37 °C with shaking. Then, the digestion mixture was removed and peptides were extracted from the gel using water/MeCN with 5 % (*v/v*) formic acid.

The digested samples were separated using a nanoAcquity Ultra Performance Liquid Chromatograph (UPLC, Waters, Milford, MA, USA) on a Waters ACQUITY UPLC M-Class Peptide C18 (130 Á, 1.78 μm, 75 μm × 250 mm) column, with a 45-min gradient. The eluents were water (A) and acetonitrile containing 0.1% (*v/v)* formic acid (B) at a flow rate of 0.35 μL min^{-1} using an LC gradient (3 %–40 % (*v/v*) B). The LC was coupled to a high-resolution Q Exactive Plus quadrupole-orbitrap hybrid mass spectrometer (Thermo Fisher Scientific) using the Data Dependent Acquisition method. Overall, the MS data were assessed with MaxQuant software (https://maxquant.org/maxquant/) [26] using the UniProt *C. albicans* SC5314 FASTA file (https://www.uniprot.org/proteomes/UP000000559) [27].

2.9. In silico protein–protein docking and protein sequence alignment

To visualize the interaction between NFAP2 and its interacting

partner, virtual protein–protein docking experiments were conducted with the HADDOCK2.4 web server using the blind docking function [28]. For this analysis, the AlphaFold structures of the identified NFAP2-interacting proteins were downloaded from the UniProt database as receptors [27]. The experimentally (nuclear magnetic resonance spectroscopy) determined NFAP2 structure as a ligand was applied [29]. Prior to the *in silico* protein–protein docking, the reliability of the AlphaFold protein structures was examined using the Ramachandran plot analysis function of MolProbity [30]. The results of the docking were visualized with Chimera vers. 1.16 [31]. The amino acid sequences of the interacting proteins and their human orthologs (downloaded from the UniProt database) [27] were aligned with Clustal Omega [32] and visualized with BioEdit [33].

2.10. Data availability

The raw sequencing reads and read counts were uploaded to the NCBI Gene Expression Omnibus database under the accession number (GSE290357) [34].

3. Results

3.1. Internalization of NFAP2 in C. albicans

In our previous studies, we revealed that when NFAP2 is applied at the minimum inhibitory concentration (MIC), it exerts a rapid, cytocidal, antifungal effect on *C. albicans* through plasma membrane disruption [15,20]. However, observations in this study indicate that when NFAP2 is applied at concentrations below the MIC (< 6.25 μg mL^{-1} to 1 × 10^5 cells in LCM), the plasma membrane of *C. albicans* remains intact and NFAP2 is localized within the cells. In order to characterize this phenomenon, we followed the Bd-NFAP2 internalization in *C. albicans* over time using CLSM. PI co-staining was performed to reveal the consequent cell death. After 30 min of treatment at a concentration of 3.125 μg mL^{-1} Bd-NFAP2, cell surface, internal and vacuolar localization of Bd-NFAP2 was observed. After 1 and 2 h, NFAP2 localized exclusively in the cytoplasm. Significant cell death was not observed after 4 h of treatment (Fig. 1).

To quantify the proportion of the NFAP2-internalization consequent to cell death, FACS analysis was conducted with two concentrations of Bd-NFAP2 (7.5 μg mL^{-1} and 15 μg mL^{-1} to 2 × 10^6 cells in LCM). Based on the results, 39 % and 56 % of the *C. albicans* cells bind or take up NFAP2, respectively, while only 12 % and 13 % of them were dead at respective concentrations, after 6 h of treatment (Table 1). Table S1 provides a detailed summary of the statistical analysis results. All these results indicate that NFAP2 below the MIC can exert a slow antifungal effect by inhibiting key cellular functions *via* interactions with intracellular target(s) in *C. albicans*.

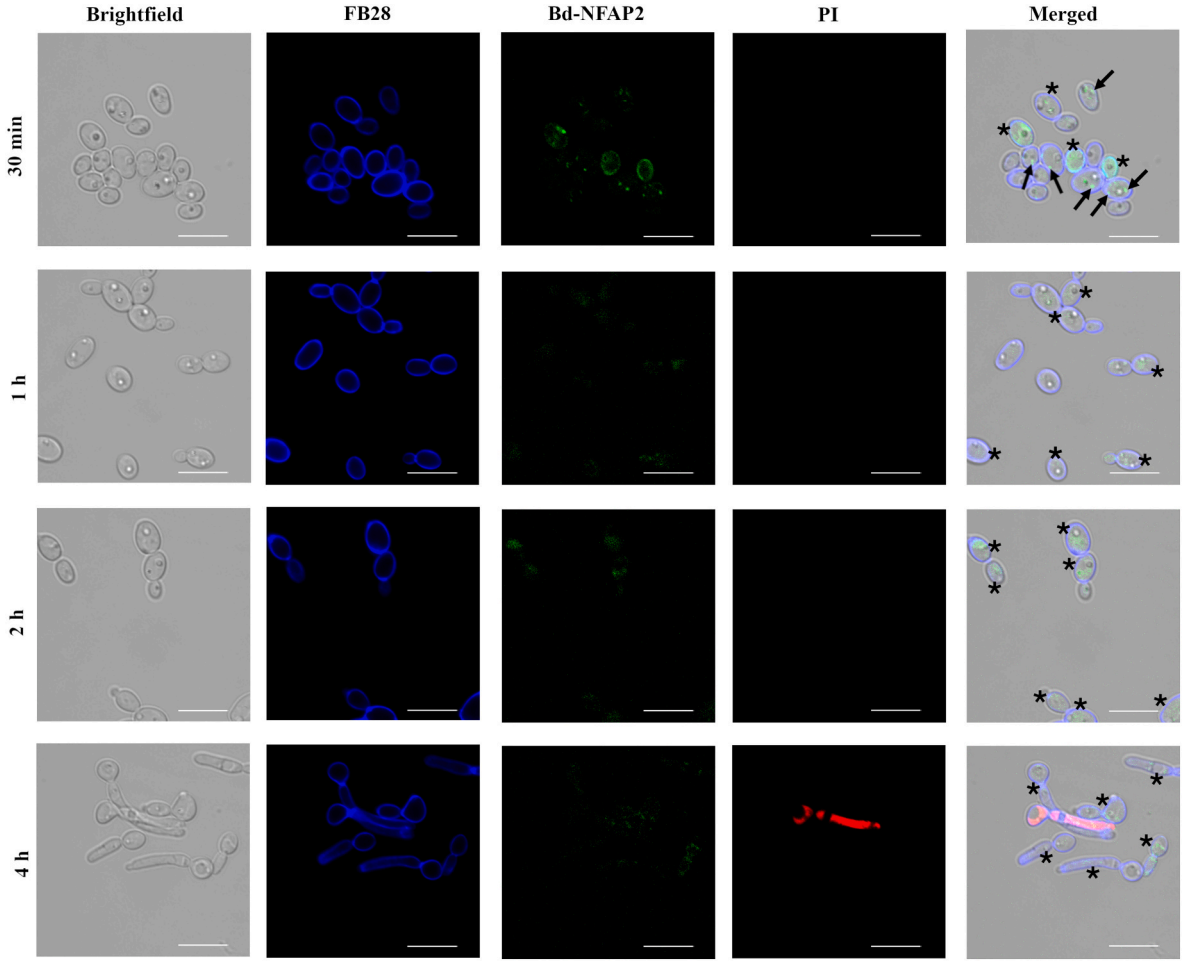

Fig. 1. Confocal laser scanning microscopy analysis of NFAP2 internalization in *Candida albicans* SC5314. *C. albicans* cells (2 × 10^6 cells) were treated with 3.125 μg mL^{-1} Bd-NFAP2 (green fluorophore boron-dipyrromethene-labeled NFAP2) for 30 min, 1 h, 2 h, and 4 h, followed by staining with a fluorescent brightener (FB28, 5 μg mL^{-1}) and propidium-iodide (PI, 5 μg mL^{-1}). Arrows indicate the vacuolar localization of NFAP2, while asterisks mark its internal (cytoplasmic) localization. A representative image from three independent experiments is presented. Scale bar: 10 μm. (For interpretation of the references to colour in this figure legend, the reader is referred to the web version of this article.)

Table 1
FACS analysis of Bd-NFAP2 binding and internalization in *C. albicans* SC5314.

	PI+ %	Bd-NFAP2+ %	Double + %	all Bd-NFAP2 + %
Untreated	10.21 ± 3.37	0.12 ± 0.17	0.18 ± 0.21	0.3 ± 0.38
Bd-NFAP2-treated (7.5 μg mL^{-1})	1.98 ± 2	26.5 ± 16.97	12.38 ± 9.35	38.88 ± 26.32
Bd-NFAP2-treated (15 μg mL^{-1})	0.58 ± 0.007	42.85 ± 13.08*	13.35 ± 3.74	56.2 ± 16.82*

Bd-NFAP2: BODIPY-labeled NFAP2, PI+: proportion of PI+ cells, Bd-NFAP2+: proportion of Bd-NFAP2+ cells, Double+: proportion of PI+ cells in the Bd-NFAP2+ population, all Bd-NFAP2 + %: Bd-NFAP2+ and Double+. * indicate significance difference between 7.5 μg mL^{-1} and 15 μg mL^{-1} Bd-NFAP2 treated samples, *p*-value <0.05 and show a medium effect size. Detailed statistical analysis is provided in Table S1.

3.2. Growth rate of C. albicans in the presence of NFAP2

In order to prove the assumption for a slow antifungal effect of NFAP2 when it is applied below the MIC, the cell density of the NFAP2-treated cultures (7.5 μg mL^{-1}, 15 μg mL^{-1} and at MIC) was monitored over time and compared with that of the untreated culture. Treatment with NFAP2 at the MIC (200 μg mL^{-1}) and 15 μg mL^{-1} influenced the growth rate of *C. albicans*. Moreover, the cell density (OD_{600}) in the presence of NFAP2 remained constant for 6 h, while a continuous increase was observed in the presence of 7.5 μg mL^{-1} NFAP2 and in its absence (Fig. 2A). To evaluate the fungicidal effect of NFAP2 at its MIC, each culture was subjected to a fivefold serial dilution and spotted onto YPD agar plates. The culture treated with the MIC concentration showed markedly reduced growth compared to cultures treated with lower concentrations (15 μg mL^{-1} and 7.5 μg mL^{-1}) and the untreated control, indicating a loss of viability at MIC (Fig. 2B). These results suggest physiological changes in *C. albicans* under NFAP2 pressure.

3.3. Impact of NFAP2 treatment on the transcriptome of C. albicans

To gain insights into the potential physiological changes in *C. albicans* in the presence of NFAP2 below the MIC, the transcriptome of the NFAP2-treated (15 μg mL^{-1}) *C. albicans* cells was compared with that of the untreated cells. In order to obtain a representative, high-quality, non-degraded transcriptome, RNA sampling of the NFAP2-treated culture was performed when the majority of the cells took up NFAP2, but the consequent cell death was minimal. FACS analysis revealed that this time was after six h of incubation (Table 1). Considering that NFAP2 treatment impacts the growth rate of *C. albicans* culture (Fig. 2), for a reliable comparison RNA was isolated from an untreated culture with an equal cell density to that of the NFAP2-treated culture because the transcriptome profile can be altered at different growth phases. According to the growth curves, the two-hours-old untreated *C. albicans* culture showed an equal cell density to that of the six-hours-old NFAP2-treated culture (Fig. 2).

Principal component analysis (PCA) indicated that NFAP2 treatment induced transcriptomic changes in *C. albicans* (Fig. S1A). The NFAP2-treated samples exhibited tight clustering, distinctly separating from the untreated control samples. This clear segregation underscored the substantial impact of NFAP2 on the gene expression profile of *C. albicans*, leading to significant transcriptomic alterations.

Further, a comparison of the global expression profiles between the NFAP2-treated and untreated cells revealed 474 differentially expressed genes (DEGs). Among them, 191 genes were upregulated, whereas 283 genes were downregulated, in response to NFAP2 treatment (log_2 fold-change: > 1.5 or < -1.5, $p < 0.05$) (Fig. S1B, Supplementary File 1). The transcriptional responses to NFAP2 were further characterized by conducting functional enrichment analyses of GO terms [35,36] and KEGG pathways [37].

The GO enrichment analysis of upregulated genes (Fig. 3) revealed numerous terms in the biological process category, including: hyphal growth, G1/S transition of the mitotic cell cycle, regulation of cyclin-dependent protein serine/threonine kinase activity, negative regulation of filamentous growth, fungal-type cell wall organization, protein phosphorylation, the lipid metabolic process, flocculation, filamentous growth of a population of unicellular organisms in response to starvation, cellular response to starvation, regulation of gene expression, the cell wall chitin biosynthetic process, protein glycosylation, nucleosome assembly, mitotic cell cycle phase transition, rRNA transcription, filamentous growth, and regulation of the cell cycle (Fig. 3, Supplementary File 2). In the molecular function category, the upregulated terms included: the structural constituent of chromatin, cyclin-dependent protein serine/threonine kinase regulator activity, protein kinase activity, protein heterodimerization activity, DNA binding, and protein serine kinase activity (Fig. 3, Supplementary File 2). For the cellular component category, the enriched terms for the upregulated genes were nucleosome, hyphal cell wall, cyclin-dependent protein kinase holoenzyme complex, side of membrane, yeast-form cell wall, cell surface,

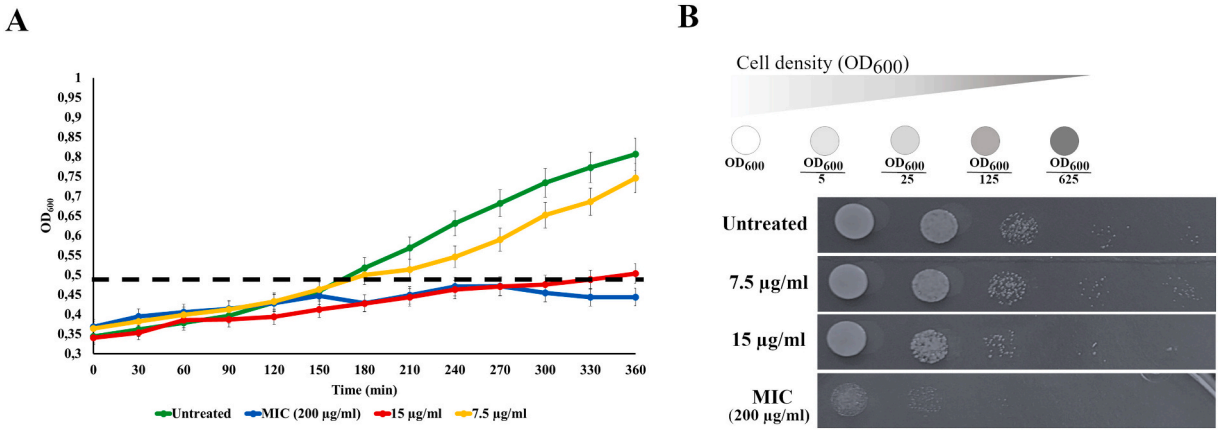

Fig. 2. Effect of NFAP2 on the growth rate of *Candida albicans* SC5314. The untreated control is shown in green, the MIC-treated (200 μg mL^{-1}) culture in blue, 15 μg mL^{-1} NFAP2-treated culture in red, and 7.5 μg mL^{-1} NFAP2-treated culture in orange. The dashed line indicates the equal cell density of the NFAP2-treated cultures (15 μg mL^{-1}) to that of the untreated ones (A). Growth ability of the untreated and NFAP2-treated (200 μg mL^{-1} [MIC], 15 μg mL^{-1}, 7.5 μg mL^{-1}) cultures on YPD agar plate (B). (For interpretation of the references to colour in this figure legend, the reader is referred to the web version of this article.)

extracellular region, nucleus, centrosome, plasma membrane, nucleoplasm, extracellular vesicle, cellular bud neck, cell periphery, nucleolus, fungal-type cell wall, Golgi apparatus, and pre-ribosome large subunit precursor (Fig. 3, Supplementary File 2). The most significantly enriched KEGG pathways for upregulated genes were the cell cycle and mitogen-activated protein kinase (MAPK) signaling pathways (Fig. 3, Supplementary File 2).

The functional enrichment analyses of the downregulated genes revealed that significant biological processes, molecular functions, cellular components, and KEGG pathways are impacted by NFAP2 (Fig. 4). In the biological process category, the most significantly downregulated terms included the leucine biosynthetic process, organic substance transport, transmembrane transport, carbohydrate transport, amino acid transmembrane transport, cellular response to heat, the valine biosynthetic process, the glycolytic process, glycerophosphodiester transport, trehalose metabolism in response to stress, the arginine biosynthetic process *via* ornithine, the arginine biosynthetic process, carboxylic acid transport, the trehalose biosynthetic process, the branched-chain amino acid biosynthetic process, the glycine catabolic process, the galactose catabolic process, tetrahydrofolate interconversion, transsulfuration, and the glutamine metabolic process (Fig. 4, Supplementary File 2).

For the molecular function category, the most significantly downregulated GO terms included amino acid transmembrane transporter activity, carbohydrate:proton symporter activity, pyridoxal phosphate binding, glucose transmembrane transporter activity, acid phosphatase activity, trehalose-phosphatase activity, the alpha,alpha-trehalose-phosphate synthase (UDP-forming) activity, glycerophosphodiester transmembrane transporter activity, metal ion binding, organic anion transmembrane transporter activity, carboxylic acid transmembrane transporter activity, copper ion binding, NAD binding, and transmembrane transporter activity (Fig. 4, Supplementary File 2). The cellular component category showed downregulation in terms of the plasma membrane, cytosol, mitochondrion, fungal biofilm matrix, the

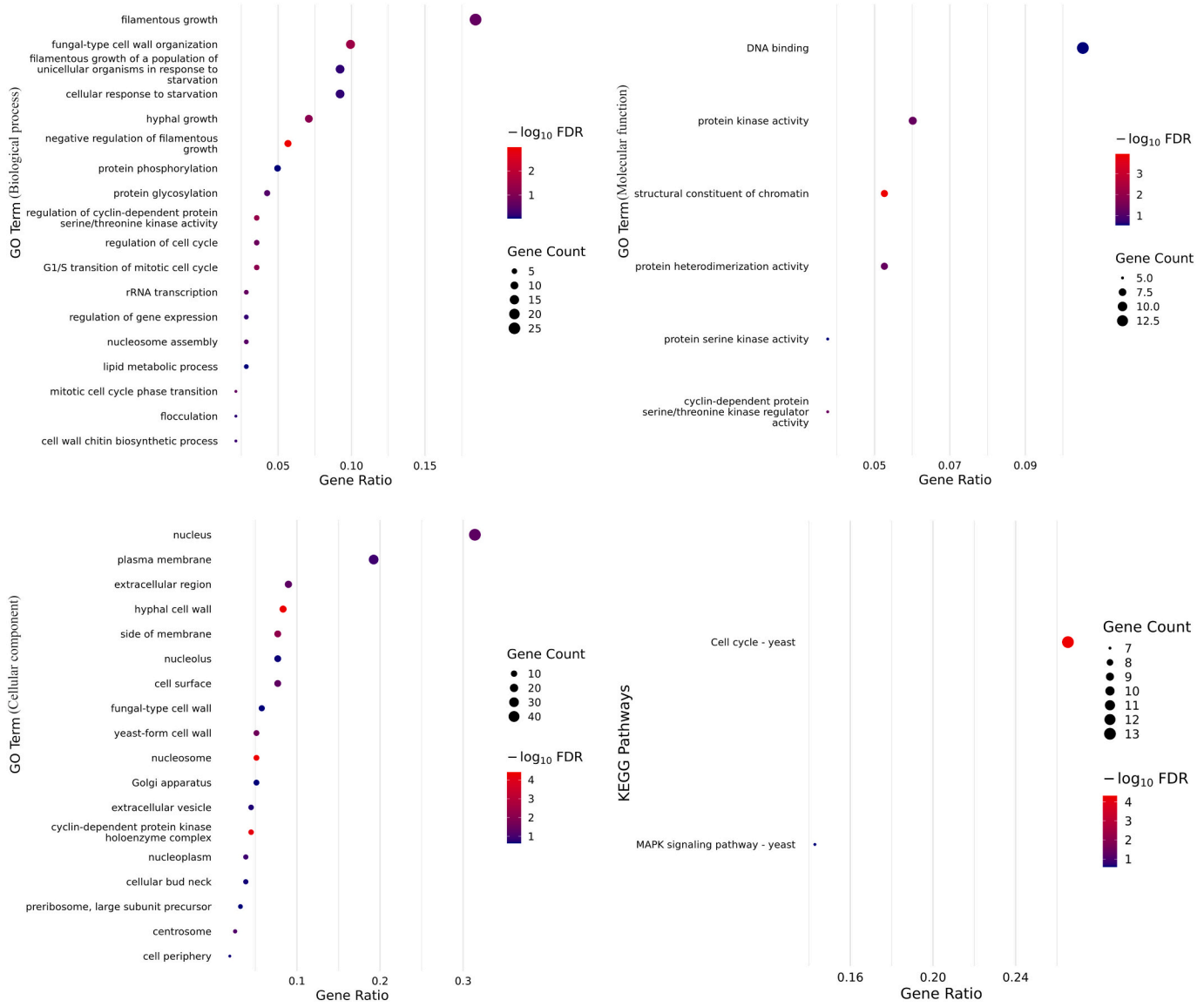

Fig. 3. Gene Ontology (GO) enrichment and Kyoto Encyclopedia of Genes and Genomes (KEGG) pathway analysis of upregulated differentially expressed genes (DEGs) in NFAP2-treated *Candida albicans* SC5314 cells. Bubble plots show enriched biological process- (top left), molecular function- (top right), cellular component terms (bottom left) and KEGG pathways (bottom right). The x-axis represents the Gene Ratio (the ratio of DEGs associated with a term/pathway relative to the total number of DEGs), while the size of each bubble indicates the number of DEGs (Gene Count) involved in that term or pathway. The colour gradient represents the statistical significance of enrichment based on the negative log10-transformed false discovery rate ($-\log_{10}$ FDR), with red indicating more significant terms. (For interpretation of the references to colour in this figure legend, the reader is referred to the web version of this article.)

alpha,alpha-trehalose-phosphate synthase complex (UDP-forming), cell surface, cell wall-bounded periplasmic space, yeast-form cell wall, and fungal-type cell wall (Fig. 4, Supplementary File 2). Enrichment analysis of KEGG pathways revealed significant downregulation in terms of the biosynthesis of amino acids; the biosynthesis of secondary metabolites; metabolic pathways; oxocarboxylic acid metabolism; valine, leucine, and isoleucine biosynthesis; carbon metabolism; arginine biosynthesis; galactose metabolism; glycolysis/gluconeogenesis; alanine, aspartate, and glutamate metabolism; methane metabolism; fructose and mannose metabolism; one carbon pool by folate; biosynthesis of cofactors; vitamin B6 metabolism; pyruvate metabolism; cysteine and methionine metabolism; starch and sucrose metabolism; pantothenate and CoA biosynthesis; and glyoxylate and dicarboxylate metabolism (Fig. 4, Supplementary File 2).

In sum, the aforementioned transcriptomic changes indicate that NFAP2 inhibits the metabolism and influences the cell division and filamentation of *C. albicans*.

3.4. Intracellular protein targets of NFAP2 in C. albicans

In order to identify the direct intracellular protein targets of NFAP2 behind the observed transcriptomic changes and involvement in the antifungal mechanism, an *in vivo* protein–protein interaction analysis was performed. *C. albicans* cells were treated with NFAP2 at a concentration below the MIC (50 μg mL^{-1} to 2×10^9 cells mL^{-1} in LCM). After the cellular internalization of NFAP2, the protein–protein interactions were stabilized with the cross-linker SDAD, which stabilizes all types of interactions between NFAP2 and its protein interaction partners by forming covalent bonds between them. Following the extraction of the total soluble proteins and subsequent Protein G enrichment, proteins were separated with SDS-PAGE (Fig. 5A). Under the aforementioned procedures, the covalently bound interacting proteins remained together, which enabled the visualization of NFAP2-interacting protein bands on the gel with immunoblotting. Western blotting experiments with NFAP2-specific antiserum indicated its high specificity (Fig. 5B).

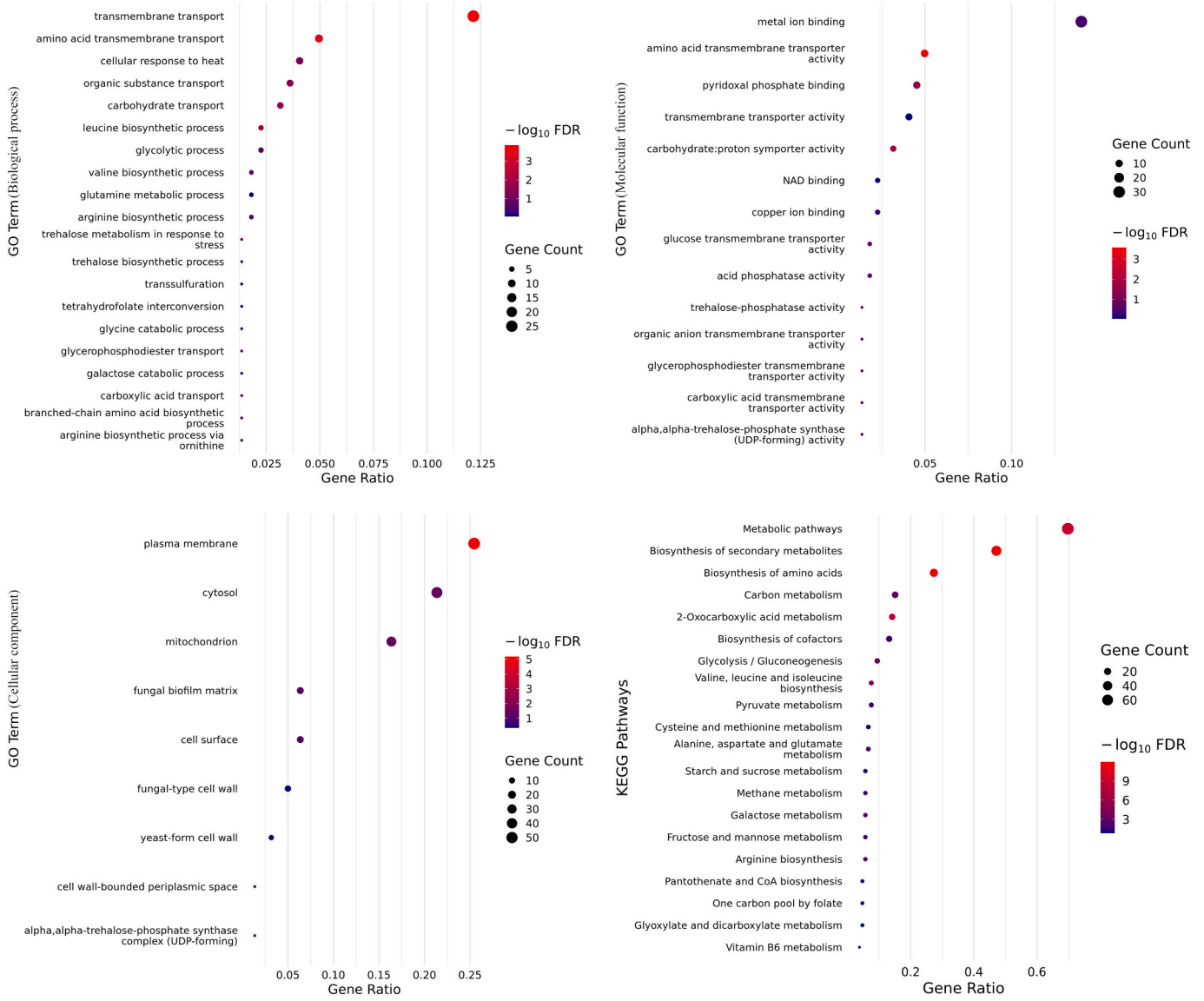

Fig. 4. Gene Ontology (GO) enrichment and Kyoto Encyclopedia of Genes and Genomes (KEGG) pathway analysis of downregulated differentially expressed genes (DEGs) in NFAP2-treated *Candida albicans* SC5314 cells. Bubble plots show enriched biological process- (top left), molecular function- (top right), cellular component terms (bottom left) and KEGG pathways (bottom right). The x-axis represents the Gene Ratio (the ratio of DEGs associated with a term/pathway relative to the total number of DEGs), while the size of each bubble indicates the number of DEGs (Gene Count) involved in that term or pathway. The colour gradient represents the statistical significance of enrichment based on the negative log10-transformed false discovery rate ($-\log_{10}$ FDR), with red indicating more significant terms. (For interpretation of the references to colour in this figure legend, the reader is referred to the web version of this article.)

MS analysis was also performed to identify the protein interaction partners of NFAP2 in the NFAP2-specific bands that were enriched, in comparison with the total protein extract before Protein G purification, and the flow through of the first washing step (Fig. 5B). Finally, three protein bands at molecular weight, *i.e.*, ~70 kDa, ~60 kDa, and ~ 55 kDa, were subjected to MS analysis for identification (Fig. 5A). Hits were considered reliable if the molecular weight fell within the range determined by SDS-PAGE, and they demonstrated the highest relative enrichment intensity, and they had sufficient sequence coverage. Based on these criteria, the glutamate decarboxylase (Gad1p; Mw: 63.884 kDa, 3.8×10^8 enrichment intensity, 60 % coverage; UniProt ID: A0A1D8PF79), the ATP synthase subunit alpha (Atp1p; Mw: 58.984 kDa, 3.7×10^8 enrichment intensity, 43.4 % coverage; UniProt ID: A0A1D8PDC4), and the enolase 1 (Eno1p; Mw: 47.1 kDa, 2.43×10^9 enrichment intensity, 61.3 % coverage; UniProt ID: P30575) were identified from the UniProt database as potential intracellular protein targets of NFAP2. The data from the MS analysis are provided in Supplementary File 3.

3.5. Characterization of the interactions between NFAP2 and its intracellular protein targets

In order to characterize the interactions between NFAP2 and its potential intracellular protein partners, *in silico* dockings were performed using the HADDOCK 2.4 server [28]. The experimentally determined structure of NFAP2 [29] and the AlphaFold-predicted structures of the interacting proteins were utilized. Specifically, the HADDOCK 2.4 server organizes the predicted models into clusters and assigns each cluster a HADDOCK score. Clusters with a score of approximately −100 are considered acceptable, while another key metric, *i.e.*, the *Z*-score, must be negative for the cluster to be valid. The model with the highest fraction of common contacts value and the lowest interface root mean square deviation value was chosen from the selected cluster to visualize the interactions (Table S2). The selected models and the amino acid residues in the interactions are presented in Fig. 6A.

Overall, the interaction analyses revealed a distinct NFAP2 binding pocket on *C. albicans* Gad1p, Atp1p, and Eno1p (Fig. 6A), whereas the target-interacting amino acid residues of NFAP2 were localized in the first part of the highly flexible N-terminus, the last part of the rigid C-terminus, and between the first two β-strands (Fig. 6B). Interestingly, the SER4, SER30, and ASP31 residues of NFAP2 appear to be involved in the interactions with all three protein targets, while THR3, TYR6, HIS26, GLY28, PRO29, LYS32, and GLN43 were involved in the interactions with two protein targets (Fig. 6B). Although these residues may represent the potential active sites of NFAP2 playing a role in its antifungal mechanism, further analysis (*e.g.*, site-directed amino acid mutation) is necessary to prove this assumption.

4. Discussion

AFPs from filamentous ascomycetes show significant potential in the treatment of *Candida* infections. To date, several studies have demonstrated that these proteins are highly active against various *Candida* species *in vitro* and *in vivo*, without harmful effects on mammalian cells [11,16]. Despite these advantages, their exact mode of action is not fully understood, hindering their therapeutic application [11,14].

According to the literature, AFPs secreted by *P. chrysogenum* (*viz.* PAF, PAFB, PAFC) are internalized by *Candida* cells through an energy-dependent mechanism. Once released from the vacuoles, intracellular reactive oxygen species are produced, triggering cell death [14]. Additionally, PeAfpA from *Penicillium expansum* can be internalized by *Saccharomyces cerevisiae* through both energy-dependent and energy-independent mechanisms. This internalization activates key signaling cascades, including the cell wall integrity pathway and cAMP-PKA signaling [38]. Although these mechanisms have been well-elucidated, direct molecular targets are not yet to be identified for ascomycetous AFPs; only their associated cellular responses have been described. To address this gap, in the present study, we characterized the antifungal mechanism of NFAP2 at the transcriptome level in *C. albicans* and examined the direct protein targets of NFAP2.

In the presence of NFAP2, significant reductions in the expression of genes involved in various transport processes, including glycerophosphodiester, organic substance, amino acid, and carbohydrate transport, as well as metabolic pathways, such as secondary metabolite biosynthesis, amino acid synthesis, and glycolysis, were observed (Fig. 4 and Supplementary File 2). These responses indicate that NFAP2 treatment decreases glucose uptake and metabolism in *C. albicans*. For

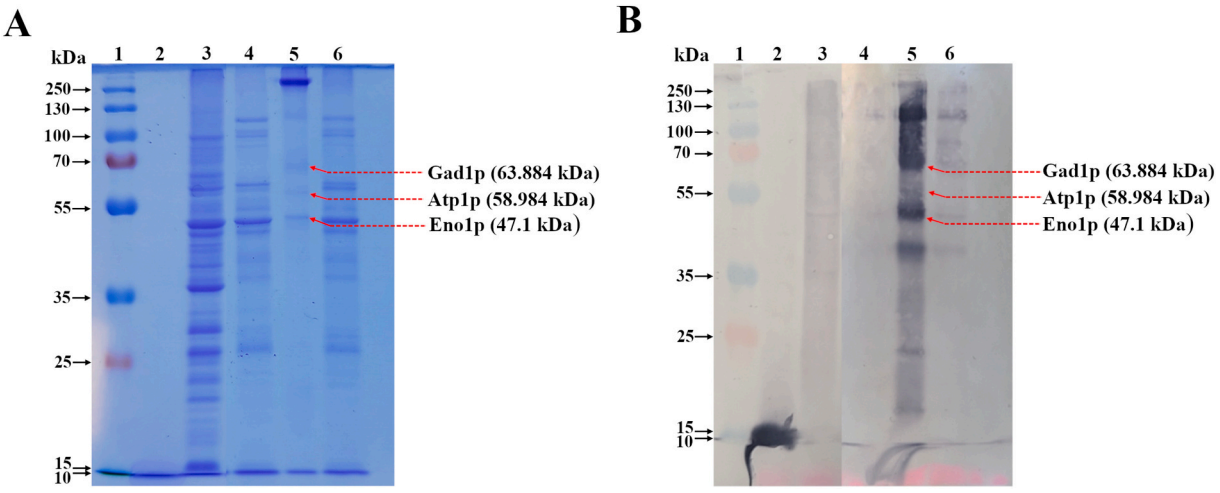

Fig. 5. SDS-PAGE (A) and immunoblot (B) analysis of *Candida albicans* SC 5314 protein extracts treated with NFAP2 and the cross-linker SDAD (succinimidyl 2-(4,4′-azipentanamido)ethyl-1,3′-dithiopropionate), which forms covalent bonds between NFAP2 and its interaction proteins. NFAP2-untreated *C. albicans* SC 5314 protein extract served as a control to exclude non-specific Protein G Plus-Agarose interaction and antibody binding. The red arrows indicate NFAP2-target protein complexes submitted to MS analysis for identification. 1: Thermo Scientific™ PageRuler™ Plus Prestained Protein Ladder (10–250 kDa), 2: NFAP2 (2 μg) as a positive control for immunoblotting, 3: *C. albicans* SC5314 intracellular total protein extract, 4: *C. albicans* SC5314 intracellular total protein extract treated with NFAP2-SDAD, 5: Protein G-enriched *C. albicans* SC5314 intracellular total protein extract treated with NFAP2-SDAD, 6: Flow through of Protein G-enriched *C. albicans* SC5314 intracellular total protein extract treated with NFAP2-SDAD. (For interpretation of the references to colour in this figure legend, the reader is referred to the web version of this article.)

A

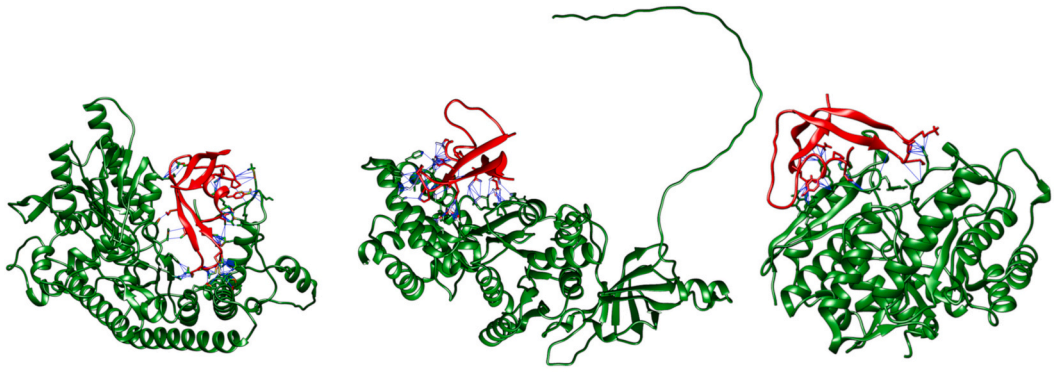

Glutamate decarboxylase

NFAP2	Glutamate decarboxylase
THR3	CYS192
SER4	GLU449
TYR7	HIS466
ASN10	PRO469
CYS11	ASN472
PRO12	GLU475
LYS16	GLU528
HIS26	HIS531
PRO29	LYS532
SER30	LYS546
ASP31	GLU547
LYS32	HIS550
VAL35	ASP553
SER37	ASN554
	GLY557
	SER558
	LYS559
	ASN560
	LYS562

ATP synthase subunit alpha

NFAP2	ATP synthase subunit alpha
THR3	GLU391
SER4	GLU393
TYR6	GLY406
HIS26	LEU407
SER27	VAL409
GLY28	SER410
PRO29	ARG411
SER30	GLY413
ASP31	LEU430
LYS34	GLN434
ILE36	ARG436
GLN43	GLU437
ASN48	ALA439
ILE50	ALA440
	PHE441
	GLN443
	PHE444

Enolase 1

NFAP2	Enolase 1
SER4	ARG10
PRO5	TYR11
TYR6	VAL12
GLY28	TYR13
SER30	ASP14
ASP31	ARG16
LYS32	ARG33
GLN43	ASN209
GLY44	VAL210
GLN46	

B

NFAP2: IATSPYYACNCPNNCKHKKGSGCKYHSGPSDKSKVISGKCEWQGGQLNCIAT
NFAP2-G: IATSPYYACNCPNNCKHKKGSGCKYHSGPSDKSKVISGKCEWQGGQLNCIAT
NFAP2-A: IATSPYYACNCPNNCKHKKGSGCKYHSGPSDKSKVISGKCEWQGGQLNCIAT
NFAP2-E: IATSPYYACNCPNNCKHKKGSGCKYHSGPSDKSKVISGKCEWQGGQLNCIAT

Fig. 6. Modeling of the interactions between NFAP2 (red) and its intracellular protein targets in *Candida albicans* SC5314 (green). Hydrogen bonds are presented in blue. The amino acid residues involved in the interactions are shown in the tables below the models (A). Secondary and primary structures of NFAP2. The red letters indicate the amino acids involved in the interaction with glutamate decarboxylase (NFAP2-G), the alpha subunit of ATP synthase (NFAP2-A), and enolase 1 (NFAP2-E) (B). (For interpretation of the references to colour in this figure legend, the reader is referred to the web version of this article.)

example, among the impacted genes in these processes, 9 out of the 20 high-affinity glucose transporters were significantly downregulated, along with several key enzymes of glycolysis, such as hexokinase 2 (HXK2), 6-phosphofructokinase subunit alpha (PFK1), 6-phosphofructokinase subunit beta (PFK2), fructose-bisphosphate aldolase (FBA1), phosphoglycerate mutase (GPM2), and the key regulator of glycolysis (TYE7), which activate the aforementioned enzymes [39,40]. These transcriptomic changes can be the consequence of the possible inhibitory effect of NFAP2 on Eno1p activity (Fig. 6A). Eno1p is a key enzyme of glycolysis, and its dysfunction can block glycolytic flux [41]. An antifungal agent baicalein exerts its effect by targeting Eno1p, which inhibits glycolysis in *C. albicans* and growth in a glucose-containing medium [42]. Yang et al. demonstrated that the expression of ENO1 is critical for cell growth in *C. albicans* [43]. The diminished efficiency of glycolysis can reduce pyruvate production [44], which is a precursor for branched-chain amino acid synthesis, and explain the downregulation of the enzymes involved in this process (Fig. 4, Supplementary File 2). The reduced availability of pyruvate and the downregulation of its metabolism may further compromise the citric acid cycle, limiting the production of intermediates required for amino acid biosynthesis (Fig. 4, Supplementary File 2) [45]. In addition, Eno1p is present in *C. albicans* biofilms, playing an important role in the colonization of the mammalian intestinal epithelium and aiding in the adhesion of yeast cells to the intestinal mucosa [46]. This also explains the downregulation of genes involved in the biofilm formation (Fig. 4, Supplementary File 2).

According to the transcriptomic data, the expression of genes associated with filamentous growth and cell cycle regulation revealed the highest upregulation (Fig. 3 and Supplementary File 2). This increased gene expression related to filamentous growth could be attributed to the interaction between Gad1p and NFAP2. Supporting this result, Reyes-García et al. have demonstrated that γ-aminobutyric acid, the product of Gad1p, increases germ-tube formation in *C. albicans* [47]. Our

internalization experiments with NFAP2 further confirmed this finding, demonstrating germ-tube formation as early as 4 h after NFAP2 treatment (Fig. 1). The upregulation of genes involved in starvation-induced filamentation can be explained by the decreased glucose transport, glycolysis, and amino acid biosynthesis and transport (Fig. 3, Fig. 4 and Supplementary File 2) [48,49]. Han et al. demonstrated that during the yeast-to-hypha transition, the primary metabolic pathway of *C. albicans* is globally downregulated [50].

Previous studies have reported that *C. albicans* shows slow growth under various stress conditions. These conditions include oxidative and osmotic stress, as well as exposure to heavy metals or antifungal agents. Under such stresses, genes related to cell cycle regulation and cell wall remodeling are upregulated, while those involved in transport, transcription, and metabolism are downregulated [51–53]. Slow growth and similar transcriptomic changes were also observed in the presence of NFAP2 (Fig. 2, Fig. 3, Fig. 4 and Supplementary File 2), which could be the consequence of the direct antifungal mechanism of NFAP2 *via* the inhibition of Gad1p and Atp1p functions. Additionally, it was found that the deletion of ATP1 elevates oxidative stress in *C. albicans* [54], whereas GAD1 is required for normal oxidative stress in *S. cerevisiae* [55,56]. The NFAP2 exposure led to the downregulation of carbohydrate metabolism-related genes (Fig. 4, Supplementary File 2), whereas oxidative stress upregulated these genes [52]. This indicates that NFAP2 may directly inhibit the function of Eno1p and suppresses glycolysis.

Protein−protein interaction analysis indicated that NFAP2 binds to Atp1p, an important component of the mitochondrial ATP synthase complex, which is responsible for the majority of cellular ATP production through oxidative phosphorylation. This process is essential for the survival and growth of the fungus [54]. The interaction of NFAP2 with Atp1p likely suppresses ATP synthase activity, potentially explaining the slower growth observed in the presence of NFAP2 (Fig. 2). This observation, along with the reduced pyruvate production caused by the decreased glycolytic flux, suggests that NFAP2 disrupts energy production in *C. albicans* at multiple levels. A previous study has shown that *C. albicans* mutants that lack ATP1 tend to exhibit impaired filamentation and biofilm formation [54], which could be connected with the observed transcriptomic changes in filamentation-related genes (Supplementary File 2).

The upregulation of cell cycle- and MAPK pathway-related genes and the downregulation of transmembrane transport genes (Fig. 3, Fig. 4 and Supplementary File 2) cannot be directly associated with the identified protein partners of NFAP2. NFAP2 may have additional protein targets, including membrane proteins, that directly regulate these processes. Furthermore, the observed upregulation and downregulation might be an indirect effect of NFAP2. Notably, it is possible that the upregulation of genes linked to the cell cycle and the MAPK pathway are associated with the yeast-to-hypha transition induced by NFAP2 treatment [57].

Giner-Llorca et al. investigated the transcriptomic changes in *S. cerevisiae* cells in response to PeAfpA. Upon comparing our transcriptomic results with those reported by Giner-Llorca et al., some similarities and some differences were observed. Functional enrichment analysis showed that, in response to both AFPs, cyclin-dependent serine/threonine kinase activity, cell wall organization, cell cycle, and the MAPK pathway were upregulated (Fig. 3) [38]. The most important difference in their transcriptomic changes is that the genes involved in filamentous growth were upregulated in *C. albicans* in response to NFAP2 (Fig. 3), whereas PeAfpA increased the expression of the genes associated with cellular bud formation in *S. cerevisiae* [38]. GO analyses indicated that both proteins negatively regulate transmembrane transport, carbon metabolism, and pyruvate metabolism, although these effects are more prominent in the case of NFAP2 (Fig. 4). Specific processes, including amino acid transport, glycerophosphodiester transport, carbohydrate transport, glycolysis, and amino acid biosynthesis/metabolism, formed distinct groups in the GO analysis of NFAP2 treatment (Fig. 4). In contrast, PeAfpA significantly reduced the expression of the genes associated with the tricarboxylic acid cycle and aerobic respiration, which was not observed in the case of NFAP2 treatment. Notably, NFAP2 reduced the expression of the genes involved in biofilm matrix formation, which is particularly relevant for its antifungal efficacy [38]. Our transcriptome analysis revealed the upregulation of the cell wall chitin biosynthetic process (chitin synthases CHS2, CHS3, CHS7), in response to NFAP2 (Fig. 3, Supplementary File 2), whereas AFP produced by *Aspergillus giganteus* also increased the expression of chitin synthase genes, especially CHS3 in *S. cerevisiae* [58].

The present study offers further evidence that NFAP2 is a promising topical therapeutic candidate for treating *Candida* infections. However, its use for the treatment of invasive candidiasis *via* intravenous administration is limited by its predicted high binding affinity to human serum albumin ($\Delta G = -12.16$ kcal/mol; Kd [dissociation constant] = 1.21e−09 M) [16]. This high binding affinity can sequester the peptide in the bloodstream, reducing its free concentration and bioavailability at the site of infection, which likely reduces its systemic efficacy. NFAP2 binding pockets in the identified interaction partners (Fig. 6A) can be employed as target for drug development to discover/design molecules that bind them with better pharmacokinetic properties, but with similar antifungal effects and fungal-specific modes of action to those of NFAP2. Our results indicate that the NFAP2-binding site on Gad1p shows low sequence homology to the human ortholog (Fig. S2), suggesting fungal specificity and low toxicity to human cells. Gad1p appears to play a role in fungal stress response and metabolic regulation, and its disruption increases the susceptibility of the cells [47,55,56]. These results indicate that Gad1p is a promising and selective antifungal target. Eno1p and Atp1p have been recognized as potential antifungal drug targets in the treatment of *C. albicans* infections owing to their essential role in energy metabolism and virulence [41,59,60]. However, Atp1p exhibits very high homology with its human orthologs, while the NFAP2 binding pocket is identical in both (Fig. S3). Although it represents a potentially good target due to its essential role in the cells [54], its high homology with human orthologs makes it unsuitable as a drug target because of the risk of toxic side effects and lack of specificity. However, the lack of harmful effects of NFAP2 on mammalian cells contradicts this assumption [11,16]. The high homology of Eno1p with its human orthologs renders it unsuitable as an antifungal drug target because it presumably imposes toxicity on the host [41]. Our molecular modeling results indicated that NFAP2 binds to a unique region of *C. albicans* Eno1p (Fig. S4), which is distinct from its human orthologs. This and the essential role of Eno1p make it a promising antifungal drug target. This is further supported by the antifungal agent baicalein, which also targets the Eno1p [42].

Beyond Eno1p and Atp1p, several studies have identified other potential drug targets against *C. albicans* [61–66]. Our findings indicated that NFAP2 treatment significantly reduced the expression of many these potential targets. For instance, PHO100, which encodes an acid phosphatase, was strongly downregulated ($\log_2$ fold-change: −7.11) [61]. Similarly, 3-isopropylmalate dehydratase (LEU1, $\log_2$ fold-change: −5.01), Na(+)-exporting P-type ATPase (ENA2, $\log_2$ fold-change: −4.92) and nitric oxide dioxygenase (YHB1, $\log_2$ fold-change: −4.69) were downregulated and recognized as potential therapeutic targets (Supplementary File 2) [62–64]. Further, downregulated genes, including alpha,alpha-trehalose-phosphate synthase (TPS1), trehalose-phosphatase (TPS2), transcription factor (CSR1), rat sarcoma virus GTPase-like protein 2 (RAS2), and FBA1, are also considered promising antifungal targets [64,65]. The products of these genes either have low homology with human orthologs, are involved in an essential pathway for *C. albicans* growth, or their loss-of-function reduces the viability and virulence of the fungus [64–66].

Summarizing the findings from our present and previous research [15–17], it appears that NFAP2 exerts a unique dual mode of action in *C. albicans* (Fig. 7). First, when NFAP2 is applied at or above MIC, it disrupts the fungal plasma membrane by selective binding to phosphatidylinositol 5-phosphate and phosphatidic acid, resulting in plasma membrane disruption and eventually cell death [20]. Second, when

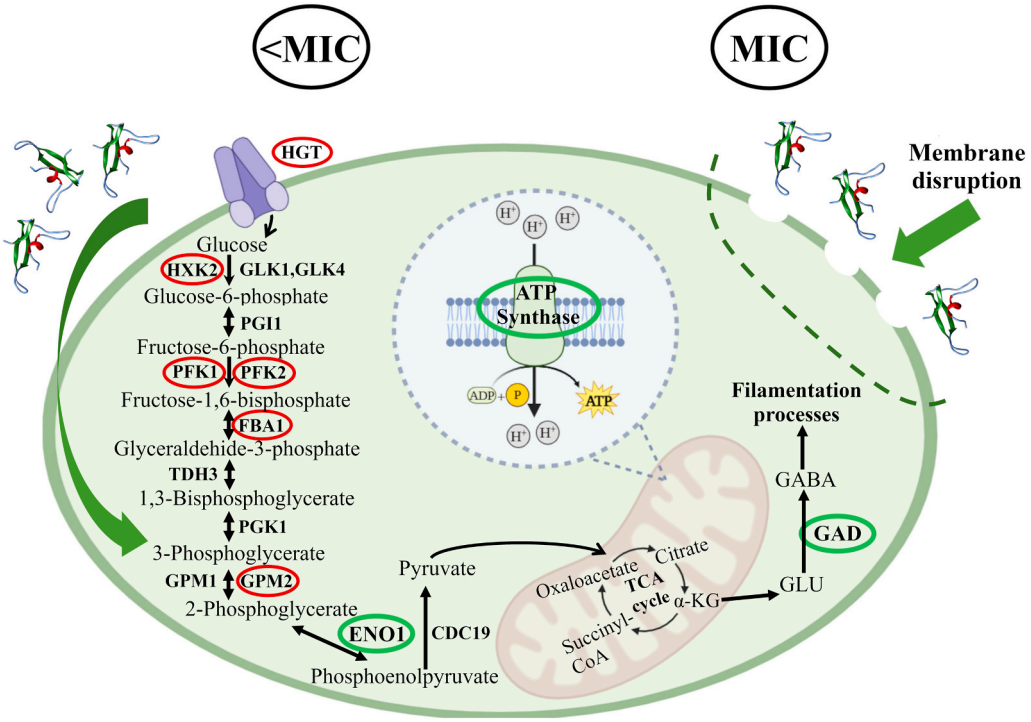

Fig. 7. Tentative model for the antifungal mechanism of NFAP2 in *Candida albicans*. When NFAP2 is applied below the minimum inhibitory concentration (<MIC), it is internalized in cells and binds its intracellular protein targets, such as glutamate decarboxylase (GAD), ATP synthase subunit alpha, and enolase 1: (ENO1), in green circles. These bindings decrease the expression of glycolytic enzymes (in red circles) and increase the gene expression in the filamentation processes. When NFAP2 is applied at the MIC, it binds to the negatively charged fungal cell membrane and disrupts the membrane [19]. (For interpretation of the references to colour in this figure legend, the reader is referred to the web version of this article.)

NFAP2 is applied below the MIC, membrane damage is not observed. In this case, NFAP2 most likely enters the cell, and it binds to Gad1p, Atp1p, and Eno1p, reducing the cellular metabolism and impacting the cell cycle and filamentation. All of these changes result in a slow growth rate.

To the best of our knowledge, this is the first study to identify the direct protein targets of an ascomycetous AFP in a yeast in relation to transcriptomic changes and provide reliable templates for antifungal drug development based on the mode of action. However, a recent study by Wang et al. (2025) demonstrated that antifungal proteins (AFPs) exhibit strong antifungal activity against the mold, *Aspergillus flavus* by interacting with the fungus-exclusive protein Ntp1. This interaction regulates multiple fungal traits and is critical for AFP binding, influencing key processes such as growth, sporulation, sclerotium formation, toxin synthesis, and pathogenicity [67].

Further experiments are required to prove the suggested antifungal mechanism of NFAP2 (*e.g.*, RT-qPCR experiments, investigation of NFAP2 target knock-out *C. albicans* mutants, *etc.*) and examine the applicability of NFAP2 targets in antifungal drug development (*e.g.*, virtual screening of drug libraries). Our findings regarding the interaction partners of NFAP2 could be validated through the use of *C. albicans* knockout mutants, as each target protein is encoded by a single, non-redundant gene. Since the genome of *C. albicans* SC5314 does not contain paralogous duplicates for these loci, gene deletion would provide definitive insights into the functional role of each protein. Given the extended time and technical complexity involved in generating such mutants, this line of investigation may be more suitable as the focus of a future study.

Supplementary data to this article can be found online at https://doi.org/10.1016/j.ijbiomac.2025.146558.

CRediT authorship contribution statement

Kinga Dán: Writing – review & editing, Writing – original draft, Visualization, Validation, Investigation, Formal analysis. **Nóra Zsindely:** Validation, Investigation, Formal analysis. **Zoltán Kele:** Validation, Investigation, Formal analysis. **Krisztián Laczi:** Validation, Methodology, Formal analysis, Data curation. **John K. Karemera:** Investigation. **Csaba Papp:** Investigation. **Attila Farkas:** Investigation. **Gergely Maróti:** Writing – review & editing, Resources. **Attila Borics:** Writing – original draft, Resources, Investigation, Funding acquisition, Formal analysis. **László Bodai:** Writing – review & editing, Resources. **László Galgóczy:** Writing – review & editing, Writing – original draft, Validation, Supervision, Resources, Project administration, Methodology, Funding acquisition, Conceptualization.

Declaration of competing interest

The authors declare that they have no known competing financial interests or personal relationships that could have appeared to influence the work reported in this paper.

Acknowledgements

K.D. holds a fellowship from ELTE Márton Áron Special College. The present work of L.G. was financed by the Hungarian National Research, Development and Innovation Office - NKFIH, FK 134343 and K 146131 projects. A.B. received funding from the Hungarian National Research, Development and Innovation Office (K 143124). The authors would like to thank Enago (www.enago.com) for the English language review. University of Szeged Open Access Fund, Grant ID: 7798.

Data availability

Data will be made available on request.

References

[1] G.D. Brown, D.W. Denning, N.A. Gow, S.M. Levitz, M.G. Netea, T.C. White, Hidden killers: human fungal infections, Sci. Transl. Med. 4 (2012) 165rv13, https://doi.org/10.1126/scitranslmed.3004404.

[2] F. Bongomin, S. Gago, R.O. Oladele, D.W. Denning, Global and multi-national prevalence of fungal diseases-estimate precision, J. Fungi (Basel) 3 (2017) 57, https://doi.org/10.3390/jof3040057.

[3] V.K. Bajpai, I. Khan, S. Shukla, P. Kumar, I.A. Rather, Y. Park, et al., Invasive fungal infections and their epidemiology: measures in the clinical scenario, Biotechnol. Bioprocess Eng. 24 (2019) 436–444, https://doi.org/10.1007/s12257-018-0477-0.

[4] D.W. Denning, Global incidence and mortality of severe fungal disease, Lancet Infect. Dis. 24 (2024) 428–438, https://doi.org/10.1016/S1473-3099(23)00692-8.

[5] A. Srinivasan, J.L. Lopez-Ribot, A.K. Ramasubramanian, Overcoming antifungal resistance, Drug Discov. Today Technol. 11 (2014) 65–71, https://doi.org/10.1016/j.ddtec.2014.02.005.

[6] J.A. Hendrickson, C. Hu, S.L. Aitken, N. Beyda, Antifungal resistance: a concerning trend for the present and future, Curr. Infect. Dis. Rep. 21 (2019) 1–8, https://doi.org/10.1007/s11908-019-0702-9.

[7] M.C. Fisher, A. Alastruey-Izquierdo, J. Berman, T. Bicanic, E.M. Bignell, P. Bowyer, et al., Tackling the emerging threat of antifungal resistance to human health, Nat. Rev. Microbiol. 20 (2022) 557–571, https://doi.org/10.1038/s41579-022-00720-1.

[8] D.V. Parums, The world health organization (WHO) fungal priority pathogens list in response to emerging fungal pathogens during the COVID-19 pandemic, Med. Sci. Monit. 28 (2022) e939088–1, https://doi.org/10.12659/MSM.939088.

[9] M. Sharma, A. Chakrabarti, Candidiasis and other emerging yeasts, Curr. Fungal Infect. Rep. 17 (2023) 15–24, https://doi.org/10.1007/s12281-023-00455-3.

[10] S. Parambath, A. Dao, H.Y. Kim, S. Zawahir, A. Alastruey-Izquierdo, E. Tacconelli, et al., *Candida albicans*-a systematic review to inform the World Health Organization fungal priority pathogens list, Med. Mycol. 62 (2024) myae045, https://doi.org/10.1093/mmy/myae045.

[11] L. Galgóczy, A. Yap, F. Marx, Cysteine-rich antifungal proteins from filamentous fungi are promising bioactive natural compounds in anti-candida therapy, Isr. J. Chem. 59 (2019) 360–370, https://doi.org/10.1002/ijch.201800168.

[12] L. Galgóczy, F. Marx, Do antimicrobial proteins contribute to overcoming the hidden antifungal crisis at the dawn of a post-antibiotic era? Microorganisms 7 (2019) 16, https://doi.org/10.3390/microorganisms7010016.

[13] N. Hegedüs, F. Marx, Antifungal proteins: more than antimicrobials? Fungal Biol. Rev. 26 (2013) 132–145, https://doi.org/10.1016/j.fbr.2012.07.002.

[14] J. Holzknecht, F. Marx, Navigating the fungal battlefield: cysteine-rich antifungal proteins and peptides from Eurotiales, Front. Fungal Biol. 5 (2024) 1451455, https://doi.org/10.3389/ffunb.2024.1451455.

[15] L. Tóth, Z. Kele, A. Borics, L.G. Nagy, G. Váradi, M. Virágh, et al., NFAP2, a novel cysteine-rich anti-yeast protein from *Neosartorya fischeri* NRRL 181: isolation and characterization, AMB Express 6 (2016) 75, https://doi.org/10.1186/s13568-016-0250-8.

[16] R. Kovács, J. Holzknecht, Z. Hargitai, C. Papp, A. Farkas, A. Borics, et al., *In vivo* applicability of *Neosartorya fischeri* antifungal protein 2 (NFAP2) in treatment of vulvovaginal candidiasis, Antimicrob. Agents Chemother. 63 (2019), https://doi.org/10.1128/AAC.01777-18 e01777-18.

[17] L. Tóth, G. Váradi, A. Borics, G. Batta, Z. Kele, Á. Vendrinszky, et al., Anti-candidal activity and functional mapping of recombinant and synthetic *Neosartorya fischeri* antifungal protein 2 (NFAP2), Front. Microbiol. 9 (2018) 393, https://doi.org/10.3389/fmicb.2018.00393.

[18] J. Holzknecht, S. Dubrac, S. Hedtrich, L. Galgóczy, F. Marx, Small, cationic antifungal proteins from filamentous fungi inhibit *Candida albicans* growth in 3d skin infection models, Microbiol. Spectr. 10 (2022) e0029922, https://doi.org/10.1128/spectrum.00299-22.

[19] G. Bende, N. Zsindely, K. Laczi, Z. Kristóffy, C. Papp, A. Farkas, et al., The *Neosartorya* (*aspergillus*) *fischeri* antifungal protein NFAP2 has low potential to trigger resistance development in *Candida albicans in vitro*, Microbiol. Spectr. 13 (2025), https://doi.org/10.1128/spectrum.01273-24 e01273-24.

[20] O. Pavela, T. Juhász, L. Tóth, A. Czajlik, G. Batta, L. Galgóczy, et al., Mapping of the lipid-binding regions of the antifungal protein NFAP2 by exploiting model membranes, J. Chem. Inf. Model. 64 (2024) 6557–6569, https://doi.org/10.1021/acs.jcim.4c00229.

[21] C. Sonderegger, L. Galgóczy, S. Garrigues, Á. Fizil, A. Borics, P. Manzanares, et al., A *Penicillium chrysogenum*-based expression system for the production of small, cysteine-rich antifungal proteins for structural and functional analyses, Microb. Cell Factories 15 (2016) 192, https://doi.org/10.1186/s12934-016-0586-4.

[22] W. da Huang, B.T. Sherman, R.A. Lempicki, Systematic and integrative analysis of large gene lists using DAVID bioinformatics resources, Nat. Protoc. 4 (2009) 44–57, https://doi.org/10.1038/nprot.2008.211.

[23] B.T. Sherman, M. Hao, J. Qiu, X. Jiao, M.W. Baseler, H.C. Lane, et al., DAVID: a web server for functional enrichment analysis and functional annotation of gene lists (2021 update), Nucleic Acids Res. 50 (2022) W216–W221, https://doi.org/10.1093/nar/gkac194.

[24] H. Wickham, ggplot2: Elegant Graphics for Data Analysis, Springer-Verlag, New York, 2016.

[25] S.F. Wong, J.W. Mak, P.C. Pook, New mechanical disruption method for extraction of whole cell protein from *Candida albicans*, Southeast Asian J. Trop. Med. Public Health. 38 (2007) 512–518.

[26] S. Tyanova, T. Temu, J. Cox, The MaxQuant computational platform for mass spectrometry-based shotgun proteomics, Nat. Protoc. 11 (2016) 2301–2319, https://doi.org/10.1038/nprot.2016.136.

[27] UniProt Consortium, UniProt: the universal protein knowledgebase in 2025, Nucleic Acids Res. 53 (2025) D609–D617, https://doi.org/10.1093/nar/gkae1010.

[28] R.V. Honorato, M.E. Trellet, B. Jiménez-García1, J.J. Schaarschmidt, M. Giulini, V. Reys et al., The HADDOCK2.4 web server: a leap forward in integrative modelling of biomolecular complexes, Nature Prot. 19 (2024) 3219–3241. doi: https://doi.org/10.1038/s41596-024-01011-0.

[29] G. Váradi, Z. Kele, A. Czajlik, A. Borics, G. Bende, C. Papp, et al., Hard nut to crack: solving the disulfide linkage pattern of the *Neosartorya* (*aspergillus*) *fischeri* antifungal protein 2, Protein Sci. 32 (2023) e4692, https://doi.org/10.1002/pro.4692.

[30] J.C. Williams, J.J. Headd, N.W. Moriarty, M.G. Prisant, L.L. Videau, L.N. Deis, et al., MolProbity: more and better reference data for improved all-atom structure validation, Protein Sci. 27 (2018) 293–315, https://doi.org/10.1002/pro.3330.

[31] E.F. Pettersen, T.D. Goddard, C.C. Huang, G.S. Couch, D.M. Greenblatt, E.C. Meng, et al., UCSF chimera-a visualization system for exploratory research and analysis, J. Comput. Chem. 25 (2004) 1605–1612, https://doi.org/10.1002/jcc.20084.

[32] F. Madeira F, N. Madhusoodanan, J. Lee, A. Eusebi, A. Niewielska, A.R.N. Tivey et al., The EMBL-EBI job dispatcher sequence analysis tools framework in 2024, Nucleic Acids Res. 52 (2024) W521–525. doi:https://doi.org/10.1093/nar/gkae241.

[33] T.A. Hall, Bioedit: a user-friendly biological sequence alignment editor and analysis program for windows 95/98/NT, Nucleic Acids Symp. Ser. 41 (1999) 95–98.

[34] T. Barrett, S.E. Wilhite, P. Ledoux, C. Evangelista, I.F. Kim, M. Tomashevsky, et al., NCBI GEO: archive for functional genomics data sets–update, Nucleic Acids Res. 41 (2013) D991–D995, https://doi.org/10.1093/nar/gks1193.

[35] M. Ashburner C.A. Ball J.A. Blake D. Botstein H. Butler J.M. Cherry et al Gene ontology: tool for the unification of biology The Gene Ontology Consortium Nat. Genet. 25 2000 25 29 https://doi.org/10.1038/75556.

[36] E. Speretta, N. Tyagi, K. Warner, R. Zaru, A.D. Diehl, R. Lee, et al., The gene ontology knowledgebase in 2023, Genetics 224 (2023) iyad031, https://doi.org/10.1093/genetics/iyad031.

[37] M. Kanehisa, S. Goto, KEGG: Kyoto encyclopedia of genes and genomes, Nucleic Acids Res. 28 (2000) 27–30, https://doi.org/10.1093/nar/28.1.27.

[38] M. Giner-Llorca, A. Locascio, J.A. Del Real, J.F. Marcos, P. Manzanares, Novel findings about the mode of action of the antifungal protein PeAfpA against *Saccharomyces cerevisiae*, Appl. Microbiol. Biotechnol. 107 (2023) 6811–6829, https://doi.org/10.1007/s00253-023-12749-0.

[39] J. Fan, V. Chaturvedi, S.H. Shen, Identification and phylogenetic analysis of a glucose transporter gene family from the human pathogenic yeast *Candida albicans*, J. Mol. Evol. 55 (2002) 336–346, https://doi.org/10.1007/s00239-002-2330-4.

[40] C. Askew, A. Sellam, E. Epp, H. Hogues, A. Mullick, A. Nantel, et al., Transcriptional regulation of carbohydrate metabolism in the human pathogen *Candida albicans*, PLoS Pathog. 5 (2009) e1000612, https://doi.org/10.1371/journal.ppat.1000612.

[41] S. Wijnants, J. Vreys, P. Van Dijck, Interesting antifungal drug targets in the central metabolism of *Candida albicans*, Trends Pharmacol. Sci. 43 (2022) 69–79, https://doi.org/10.1016/j.tips.2021.10.003.

[42] L. Li, H. Lu, X. Zhang, M. Whiteway, H. Wu, S. Tan, et al., Baicalein acts against *Candida albicans* by targeting Eno1 and inhibiting glycolysis, Microbiol. Spectr. 10 (2022) e0208522, https://doi.org/10.1128/spectrum.02085-22.

[43] Y.L. Yang, H.F. Chen, T.J. Kuo, C.Y. Lin, Mutations on CaENO1 in *Candida albicans* inhibit cell growth in the presence of glucose, J. Biomed. Sci. 13 (2006) 313–321, https://doi.org/10.1007/s11373-005-9054-6.

[44] N.S. Chandel, Glycolysis, Cold Spring Harb. Perspect. Biol. 13 (2021) a040535, https://doi.org/10.1101/cshperspect.a040535.

[45] K. Jastrzębowska, I. Gabriel, Inhibitors of amino acids biosynthesis as antifungal agents, Amino Acids 47 (2015) 227–249, https://doi.org/10.1007/s00726-014-1873-1.

[46] R.C. Silva, A.C. Padovan, D.C. Pimenta, R.C. Ferreira, C.V. da Silva, M.R. Briones, Extracellular enolase of *Candida albicans* is involved in colonization of mammalian intestinal epithelium, Front. Cell. Infect. Microbiol. 4 (2014) 66, https://doi.org/10.3389/fcimb.2014.00066.

[47] M.G. Reyes-García, F. Hernández-Hernández, F. García-Tamayo, Gamma-aminobutyric acid (GABA) increases *in vitro* germ-tube formation and phospholipase B1 mRNA expression in *Candida albicans*, Mycoscience 53 (2012) 36–39, https://doi.org/10.1007/s10267-011-0130-7.

[48] A.R. Holmes, M.G. Shepherd, Proline-induced germ-tube formation in *Candida albicans*: role of proline uptake and nitrogen metabolism, Microbiology 133 (1987) 3219–3228, https://doi.org/10.1099/00221287-133-11-3219.

[49] A.R. Holmes, M.G. Shepherd, Nutritional factors determine germ tube formation in *Candida albicans*, J. Med. Vet. Mycol. 26 (1988) 127–131 (PMID: 3047355).

[50] T.I. Han, R.D. Cannon, S.G. Villas-Bôas, Metabolome analysis during the morphological transition of *Candida albicans*, Metabolomics 8 (2012) 1204–1217, https://doi.org/10.1007/s11306-012-0416-6.

[51] D.A. Smith, S. Nicholls, B.A. Morgan, A.J. Brown, J. Quinn, A conserved stress-activated protein kinase regulates a core stress response in the human pathogen *Candida albicans*, Mol. Biol. Cell 15 (2004) 4179–4190, https://doi.org/10.1091/mbc.e04-03-0181.

[52] B. Enjalbert, D.A. Smith, M.J. Cornell, I. Alam, S. Nicholls, A.J. Brown, J. Quinn, Role of the Hog1 stress-activated protein kinase in the global transcriptional

response to stress in the fungal pathogen *Candida albicans*, Mol. Biol. Cell 17 (2006) 1018–1032, https://doi.org/10.1091/mbc.e05-06-0501.
[53] J.L. Xie, L. Qin, Z. Miao, B.T. Grys, J.C. Diaz, K. Ting, et al., The *Candida albicans* transcription factor Cas5 couples stress responses, drug resistance and cell cycle regulation, Nat. Commun. 8 (2017) 499, https://doi.org/10.1038/s41467-017-00547-y.
[54] S.X. Li, Y.J. Song, Y.S. Zhang, H.T. Wu, H. Guo, K.J. Zhu, et al., Mitochondrial complex V α subunit is critical for *Candida albicans* pathogenicity through modulating multiple virulence properties, Front. Microbiol. 8 (2017) 285, https://doi.org/10.3389/fmicb.2017.00285.
[55] S.T. Coleman, T.K. Fang, S.A. Rovinsky, F.J. Turano, W.S. Moye-Rowley, Expression of a glutamate decarboxylase homologue is required for normal oxidative stress tolerance in *Saccharomyces cerevisiae*, J. Biol. Chem. 276 (2001) 244–250, https://doi.org/10.1074/jbc.M007103200.
[56] Y. Kamei, T. Tamura, R. Yoshida, S. Ohta, E. Fukusaki, Y. Mukai, GABA metabolism pathway genes, UGA1 and GAD1, regulate replicative lifespan in *Saccharomyces cerevisiae*, Biochem. Biophys. Res. Commun. 407 (2011) 185–190, https://doi.org/10.1016/j.bbrc.2011.02.136.
[57] E.W.L. Chow, L.M. Pang, Y. Wang, From Jekyll to Hyde: the yeast-hyphal transition of *Candida albicans*, Pathogens 10 (2021) 859, https://doi.org/10.3390/pathogens10070859.
[58] J.P. Ouedraogo, S. Hagen, A. Spielvogel, S. Engelhardt, V. Meyer, Survival strategies of yeast and filamentous fungi against the antifungal protein AFP, J. Biol. Chem. 286 (2011) 13859–13868, https://doi.org/10.1074/jbc.M110.203588.
[59] S.J. Leu, Y.C. Lee, C.H. Lee, P.Y. Liao, C.W. Chiang, C.M. Yang, et al., Generation and characterization of single chain variable fragment against alpha-enolase of *Candida albicans*, Int. J. Mol. Sci. 21 (2020) 2903, https://doi.org/10.3390/ijms21082903.
[60] H. Syed, M. Tauseef, Z. Ahmad, A connection between antimicrobial properties of venom peptides and microbial ATP synthase, Int. J. Biol. Macromol. 119 (2018) 23–31, https://doi.org/10.1016/j.ijbiomac.2018.07.146.
[61] J.R. Köhler, M. Acosta-Zaldívar, W. Qi, Phosphate in virulence of *Candida albicans* and *Candida glabrata*, J. Fungi 6 (2020) 40, https://doi.org/10.3390/jof6020040.
[62] F.J. Ruiz-Castilla, F.S. Ruiz Pérez, L. Ramos-Moreno, J. Ramos, *Candida albicans* potassium transporters, Int. J. Mol. Sci. 23 (2022) 4884, https://doi.org/10.3390/ijms23094884.
[63] A. Kuplińska, K. Rząd, Molecular targets for antifungals in amino acid and protein biosynthetic pathways, Amino Acids 53 (2021) 961–991, https://doi.org/10.1007/s00726-021-03007-6.
[64] R. Verma, D. Pradhan, M. Maseet, H. Singh, A.K. Jain, L.A. Khan, Genome-wide screening and *in silico* gene knockout to predict potential candidates for drug designing against *Candida albicans*, Infect. Genet. Evol. 80 (2020) 104196, https://doi.org/10.1016/j.meegid.2020.104196.
[65] Z.A. Hefny, B. Ji, I.E. Elsemman, J. Nielsen, P. Van Dijck, Transcriptomic meta-analysis to identify potential antifungal targets in *Candida albicans*, BMC Microbiol. 24 (2024) 66, https://doi.org/10.1186/s12866-024-03213-8.
[66] A. Rodaki, T. Young, A.J.P. Brown, Effects of depleting the essential central metabolic enzyme fructose-1,6-bisphosphate aldolase on the growth and viability of *Candida albicans*: implications for antifungal drug target discovery, Eukaryot. Cell 5 (2006) 1371–1377, https://doi.org/10.1128/ec.00115-06.
[67] Y. Wang, A. Wang, Y. Chen, C. Xie, H. Xu, Y. Lin Y, et al., The role of Npt1 in regulating antifungal protein activity in filamentous fungi, Nat. Commun. 16 (2025) 2850, https://doi.org/10.1038/s41467-025-58230-6.